Efficient Hydrogen Production on Crystalline-Amorphous Heterostructured Cobalt Boride-Phosphite Electrocatalyst

Jean Marie Vianney Nsanzimana[#1,2]*, Charles Otieno Ogolla[#1]*, Nastaran Farahbakhsh[2], Yilmaz Sakalli[3], Marco Hepp[1], Jonas Frohne[1], Walter Sebastian Scheld[1], Manuela S. Killian[2] & Benjamin Butz[1]

1 Micro- and Nanoanalytics Group, University of Siegen, Paul-Bonatz-Straße 9-11, 57076 Siegen, Germany
2 Chemistry and Structure of Novel Materials, Paul-Bonatz-Straße 9-11, 57076 Siegen, Germany
3 Micro- and Nanoanalytics Facility, University of Siegen, Paul-Bonatz-Straße 9-11, 57076 Siegen, Germany

[#] These authors contributed equally to this work.

* Corresponding author's email: jean.nsanzimana@uni-siegen.de, charles.ogolla@uni-siegen.de

Abstract:

Targeted phase engineering of nanomaterials through non-equilibrium synthesis strategies provides a rich platform for the development and tuning of nanostructured catalysts with outstanding properties and life-time. Unconventional phases or even complex heterostructures play a crucial role in the performance of catalysts for efficient water electrolysis. By utilizing a controlled, iterative reduction synthesis route, a tailored binder-free cobalt boride-phosphite electrode (Co_xB-[0.2]P-O) with mixed crystalline-amorphous phases is developed. The tailored cobalt chemistry, hierarchical morphology and mixed phases synergistically enhance the catalytic activity for hydrogen evolution reaction (HER). Those electrodes exhibit platinum-like HER performance with an overpotential of 33 mV at the standard current density of 10 mA cm^{-2}, with excellent intrinsic kinetics and enhanced electron transfer in an alkaline 1M KOH electrolyte. Comprehensive microstructure and spectroscopic analyses proved the success of the one-pot strategy to modulate the chemistry of cobalt by incorporating boron and phosphite. Moreover, the tailored formation of nanostructures with locally varying morphology by the co-existence of amorphous and crystalline phases on the nanometer scale is confirmed. This approach facilitates the rational design for tuning the metal boride-based catalysts' activity for hydrogen evolution by tailored chemistry of the metal active centers and thus the phase engineering of similar nanomaterials while avoiding the necessity of any post-synthesis thermal treatment processes.

1. Introduction

Electrochemical energy technologies will significantly contribute to the transition to a sustainable and carbon-neutral economy in order to decarbonize the energy sector.[1] One of the most critical scientific and technological problems is the development of a sustainable and cost-effective water splitting processes for industrial-scale production of green H_2 to facilitate the energy transition.[2] Heterogeneous catalysis is a key element of the solution.[3] Benchmark electrocatalysts with a zero HER overpotential used in low temperature water electrolysis systems are, however, based on scarce, expensive noble metals (specifically platinum group metal (PGM) catalysts).[4] This makes them economically less attractive and does not meet the requirements for the global demand of green H_2. Consequently, the development of low-cost, stable, and highly efficient hydrogen-evolving materials is of key importance to meet this demand. Earth-abundant transition metal (TM)-based materials have attracted much attention as alternative electrocatalysts, especially in alkaline electrolytes.[5] However, chemical modulation strategies of catalysts and economically viable synthesis routes to generate nanostructured materials with durable and enhanced catalytic performances are still required especially for the green hydrogen production, especially at an industrial scale.[4, 6]

A major process bottleneck, when operating in alkaline media, is the reduced kinetics due to the water-dissociation energy barrier.[7] However, alkaline water electrolysis allows the utilization of TM-based materials, which serve as PGM-free alternatives with better HER kinetics.[8] Emerging technologies such as anion-exchange membrane water electrolysis, for industrial scale water splitting, require electrocatalysts that are capable to even operate under mild alkaline conditions (less or equal to 1M KOH) or pure water.[9] To enhance the kinetics of the reduction reaction, the chemical environment of TM-based catalysts can be tailored by incorporating nonmetals and metalloid elements such as phosphorus, sulfur, nitrogen, selenium, and boron.[10] Engineering of the material's morphology, crystal structure, and catalyst support are leveraged to improve extrinsic catalytic activity of complete electrodes.[3] A careful choice of the substrate material and the design of the substrate/catalyst interface especially for highly conductive substrates is also important.[11] This enables strong adhesion and enhanced charge transfer due to extended exposure of more catalytic active sites to adsorbates promoting the HER activity and life-cycle of the electrocatalysts.[12] By combining the above strategies, earth-abundant transition metal-based catalysts are developed with high activity comparable to precious metal-based catalysts.

The TM-based borides and boron oxides, which are abundant and provide economically attractive alternatives, showed promising catalytic performance for water splitting.[13] Central to this class of materials is cobalt boride with moderate HER activity.[14] Cobalt boride (Co_xB)-based materials take advantage of the fact that Co as first-row transition metal possesses three unoccupied d-orbitals facilitating facile surface chemical interactions.[15] Metalloids such as boron and phosphorus have been known to influence the electronic configuration of the metal sites.[16] Electron-deficient borides have been employed to shift electrons towards the vacant d-orbitals of the active Co sites,[17] to beneficially affect the electron transfer between the reactant and the catalyst, and further to increase the reduction reaction kinetics.[10, 18] In amorphous Co_xB-based materials reverse electron transfer shifts electron density from B to Co thereby creating electron-rich Co sites which enhances Co interactions with protons leading to enhanced HER.[13a, 19] Incorporation of phosphorous into a Co_xB system directly modulates the electron density around cobalt atoms, which impacts electron transfer and the hydrogen interaction with the active sites.[20] Despite the considerable progress made in the development of efficient cobalt boride-based electrocatalysts, advanced synthesis strategies affording the tailored cobalt chemistry, modulation of the electronic nature of cobalt and advanced phase engineering at the nanoscale for HER are crucial.[21]

Besides the careful choice of a performant material system, the global and, more importantly, local crystal structure of the chosen system plays a significant role in determining its catalytic performance.[22] Amorphous systems inherently possess dangling bonds randomly oriented in space, which results in a higher degree of unsaturated electronic configurations.[23] Consequently, purely amorphous catalysts possess a large fraction of unsaturated active sites facilitating efficient adsorption and surface reactions at the cost of conductivity.[22-23] In contrast, crystalline phases enhance the material's intrinsic conductivity.[22, 24] It is therefore necessary to produce catalysts, which take advantage of the synergistic effect of complex heterostructures consisting of crystalline and amorphous phases at the nanoscale.[21-22, 25] TM-boride catalysts are typically synthesized via chemical reduction reactions of transition metal cations in aqueous solution using alkali metal tetrahydrides as reducing agent and a boron source to precipitate metal-borides.[17c, 26] However, this reaction is spontaneous and it is a challenge to control the final products. Such products are mostly amorphous,[27] and typically require post-thermal treatment to induce some form of crystallinity or utilize highly conductive carbon to enhance the electrocatalytic performance.[14, 28]

TM-boride-based nanomaterials, therefore, provide a suitable platform for phase engineering at the nanoscale to develop efficient HER electrocatalysts with unique chemistry, morphology, and unconventional mixed crystalline-amorphous phases using only a facile and cost-effective wet-chemical reduction process.[29]

Herein, we use an elaborate synthesis strategy to develop a series of self-supported, amorphous-crystalline (heterostructured), nanostructured cobalt boride phosphite electrocatalysts. Our synthesis technique avoids any additional energy-intensive annealing process as commonly employed to induce crystallinity in TM-boride based catalysts synthesized in an aqueous reducing solution. Moreover, it overcomes the use of binders, such as Nafion, to stabilize the catalyst, enabling improved mass transport, enhanced access to active sites, less interfacial resistance, and higher electrical conductivity without adding carbon nanomaterials. Degradation is minimized as the self-support on the utilized metal foam eliminates peeling of any powder catalyst during operation,[30] with the open-porous nickel foam (NF) facilitating efficient mass transport. Comprehensive electrochemical and structure characterization of Co_xB-O, reference $Co(OH)_2$ as well as the complex, highly performing Co_xB-[0.2]P-O samples, revealed that the enhanced catalytic activity resulted from the unique heterostructure and synergistic effects of cobalt with boron and phosphite in the electrocatalyst structure.

2. Results and discussion

2.1 Fabrication and surface chemistry analysis of self-supported electrode

The electroless preparation of a series of self-supported heterostructured cobalt boride-based electrodes is schematically shown in Fig. 1 A-H (details in Fig. S1). Highly open-porous and hollow nickel foam (NF) (Fig. 1 G, H, Fig. S2 A) is used as substrate as it allows for excellent liquid/gas transport, is chemically stable, provides high electrical conductivity and a suited surface for the catalyst fabrication/operation.[31] X-ray micro-tomography (µCT) furthermore depicts the hollow nature and thus material-saving NF due to its thin walls of the foam struts (Fig. 1 H). The facile synthesis employs an iteratively controlled chemical reduction reaction of cobalt cations (solution A: $Co(NO_3)_2{\cdot}6H_2O$) by mixtures of reducing agents in an aqueous solution (solution B: $NaBH_4$ and $NaH_2PO_3{\cdot}H_2O$). Sodium borohydride acts as the strong reaction-controlling reducing agent, while sodium phosphite is a weaker reducing agent.

This combination of reducing agents facilitates, both, the inherent formation of Co_xB-O and immediate doping by phosphite, while at a later stage, the complex amorphous-crystalline Co_xB-[0.2]P-O catalyst is formed. The cobalt source, i.e. solution A, is first adsorbed on the NF substrate (Fig. S1) and subsequently immersed in the reducing solution B. This iterative process was repeated 5 times, whereby the cobalt ions are locally reduced on the surface.[32] As a result, a dense, nanocrystalline and well-adhering seed layer on the NF is generated (intermediate state depicted in Fig. 1 C, D, Fig. S3 A) to assure mechanical long-term stability during catalyst operation (Fig. S4), good electron transport and an enhanced surface area (cf. Fig. 1 B, D). In a second synthesis step the seed-layer coated NF substrate is immersed into solution A, while solution B was slowly added. In this reactive mixture, the final active catalyst is formed on the seed layer, which is indicated by the roughened surface in Fig. 1 F (cf. Fig. 1 D, Fig. S2 C, D, Fig. S3 B details in SI). SEM-EDX analysis demonstrated the presence of Co, B, P, and O, indicating the formation of CoxB-[0.2]P-O (Fig. S5). Figure 1 further depicts $Co(OH)_2$ nanosheets as typically formed in $NaBH_4$-containing reduction reaction environments.[33] Particularly, the high energy impact of the rapid exothermic reaction on the roughened seed layer surface allows for the localized atomic-scale structural rearrangement and thus the formation of amorphous-crystalline heterostructured Co_xB-[0.2]P-O without any additional thermal treatment.

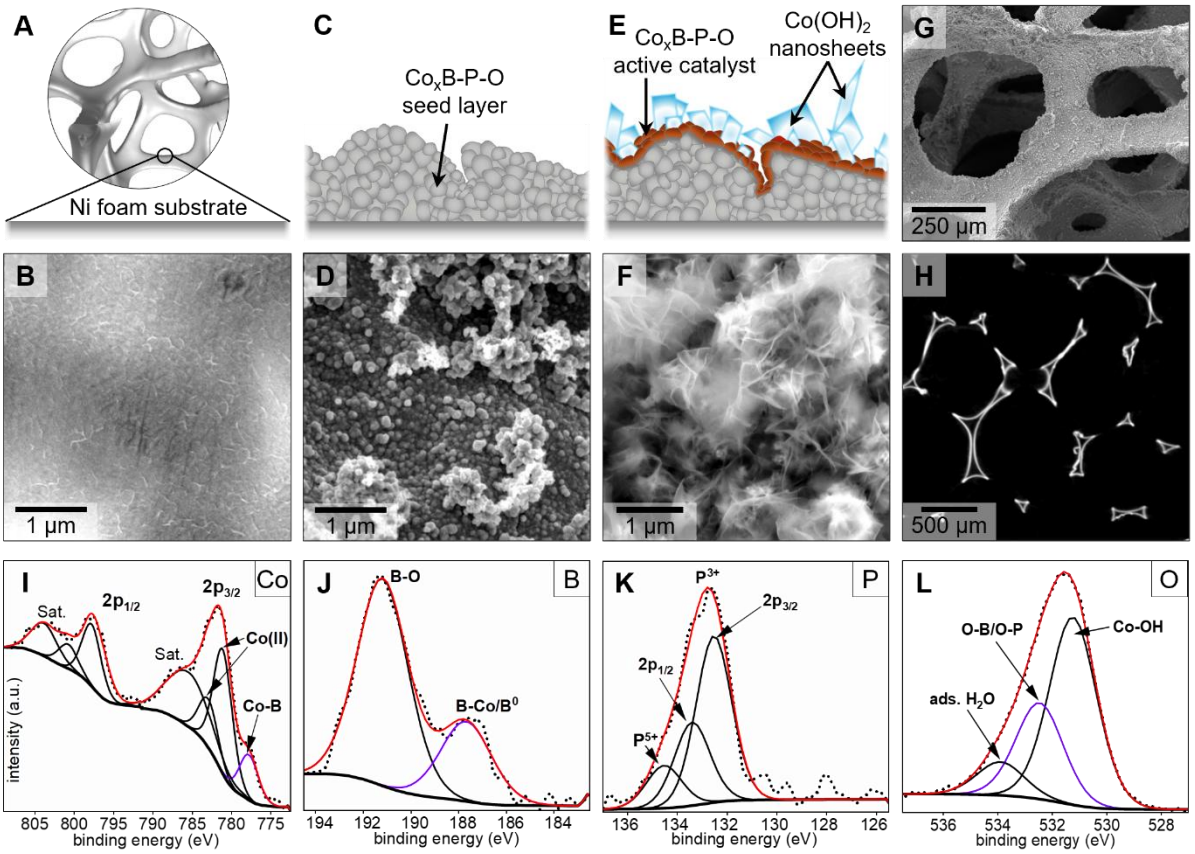

Figure 1: A-G) Electrode fabrication depicted by schematics plus representative SEM images: synthesis stages starting from clean NF surface (A,B) through intermediate step (C, D: seed layer formation) to final product (E, F: active Co_xB-[0.2]P-O catalyst with typical $Co(OH)_2$ nanosheets), G) SEM overview of high-performing electrode demonstrating complete coverage and good adhesion, H) ortho-slice (cross-section) of 3D reconstruction from µCT of hollow NF, I-L), XPS spectra of Co, B, P, and O.

Surface-sensitive X-ray photoelectron spectroscopy (XPS) (Fig.1 I-L), confirms the successful incorporation of the B and P species and their impact on the electronic environment of the Co active sites within the catalyst layer. XPS survey revealed a surface composition of 23.17 at.%, 29.71 at.%, 29.73 at.%, 5.02 at.%, and 12.37 at.% for B, C, O, P, and Co respectively (cf. Fig. S6). Deconvolution of the Co $2p_{3/2}$ spectrum clearly reveals the tailored Co-B interaction, resulting in a distinct sub-peak at 777.7 eV, which is 0.4 eV shifted to lower binding energy compared to metallic Co^0 (778.1 eV [34]) due to the electron transfer from boron to cobalt (Fig. 1 I).[17a, 17b], [17c] In addition there are two major peaks of Co $2p_{3/2}$ at 781.6 eV and Co $2p_{1/2}$ at 797.4 eV, respectively, with a spin-orbit splitting of $\Delta E = 15.8$ eV.

Detailed analysis of the Co $2p_{3/2}$ peak reveals two contributions with typical shifts to higher binding energies (781.1 eV and 782.9 eV) owing to cobalt (II) cations bound to highly electro-negative species such as hydroxides and phosphites, respectively.[14, 35] The electron transfer between Co and B is further indicated by the positive 0.6 eV shift relative to B^0 (187.1 eV) in the B 1s peak (187.7 eV), attributed to the boride species (Fig. 1 J).[17b, 28, 36] Phosphite incorporation into the catalyst was evidenced by the deconvoluted P 2p spectrum (Fig. 1 K) into two major sub-peaks at 133.6 eV and 134 eV ($\Delta = 0.87$ eV) characteristic for the presence of phosphorous (III) species and an extra peak at higher energy for phosphorous (V) in oxidized P-O molecules.[37] Like boron, the phosphorous inclusion into the Co-B system directly modulates the electron density around cobalt atoms, which impacts electron transfer and the hydrogen interaction with the active sites.[20] The O 1s spectrum (Fig. 1 L) shows three sub-peaks at 531.5 eV, 532.5 eV, and 533.9 eV. The signals at 531.5 eV and 532.5 eV consistently reveals the presence of mixed metal-oxide/hydroxide (e.g. $Co(OH)_2$/ CoO) and the P/B-O (in oxidized P species and B-O in boron-oxo species), respectively.[38]

2.2 Microstructural and chemical characterization

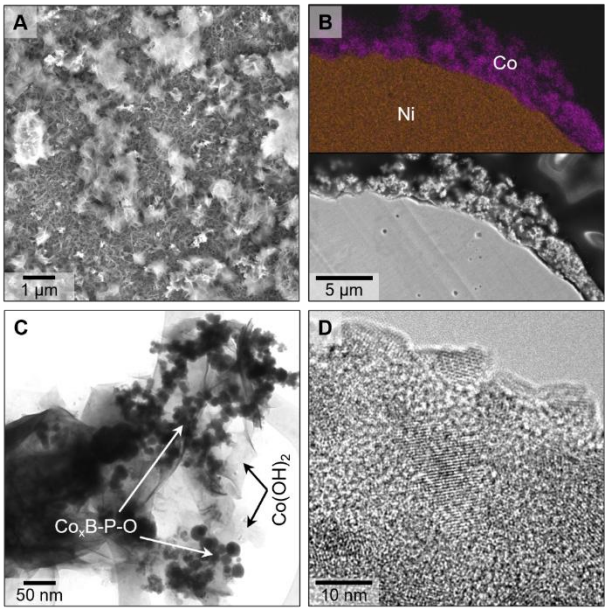

Figure 2: Morphology and microstructure of active catalyst layer**:** A) top-view SEM overview and B) cross-sectional SEM micrograph of electrode with corresponding EDXS element maps of Ni and Co, C) bright-field TEM micrograph of exposed electrode surface (scratched sample) showing internal spherical and crystalline Co_xB-[0.2]P-O nanoparticles with on-grown amorphous-crystalline catalyst heterostructure, D) HRTEM detail of active amorphous-crystalline Co_xB-[0.2]P-O heterostructure.

A comprehensive scale-bridging investigation of the microstructure, crystal structure and chemistry of the electrodes with emphasis on the active catalyst is indispensable to understand catalyst functionality, performance and long-term stability. The continuous coating of the NF surface is confirmed by SEM top-view and cross-sectional imaging (Fig. 1 F, G, Fig. 2 A, B) as corroborated by the Co mapping. The coating roughness (Fig. 2 B), governed by the seed layer with a mean grain size of the polycrystalline Co_xB-[0.2]P-O of around 100 nm (Fig. 1 D), enhances active surface area and thus promotes HER. The tailored two-step reduction reaction resulted in the formation of the targeted sequence of seed layer and active catalyst, with the latter exhibiting amorphous-crystalline morphology surpassing conventional reduction strategies with typical amorphous structure.[14] Transmission electron microscopy (TEM) confirmed the continuous coverage of the crystalline Co_xB-[0.2]P-O seed layer (and partly tiny particles generated during the second coating step) by the amorphous-crystalline catalyst heterostructure (Fig. 2 C, D).

Figure 2 D details the morphology of the amorphous-crystalline Co_xB-[0.2]P-O at the catalyst surface with crystalline domains of around 10 nm embedded in the amorphous matrix. The nanocrystalline nature of the Co_xB-[0.2]P-O particles is reflected as severe peak broadening in XRD (Fig. S7).

The complex architecture of the developed electrocatalyst is further confirmed by three-dimensional (3D) tomographic reconstruction (Fig. S13). The reconstruction delineates the nanostructures showing agglomerated nanoparticles (seed layer) at the bottom of the electrode covered by porous nanosheets at the top exposing a large surface area. This hierarchical morphology is necessary for efficient mass transport during the catalytic reaction with the large surface area providing a high number of active sites for surface chemical reactions.[39]

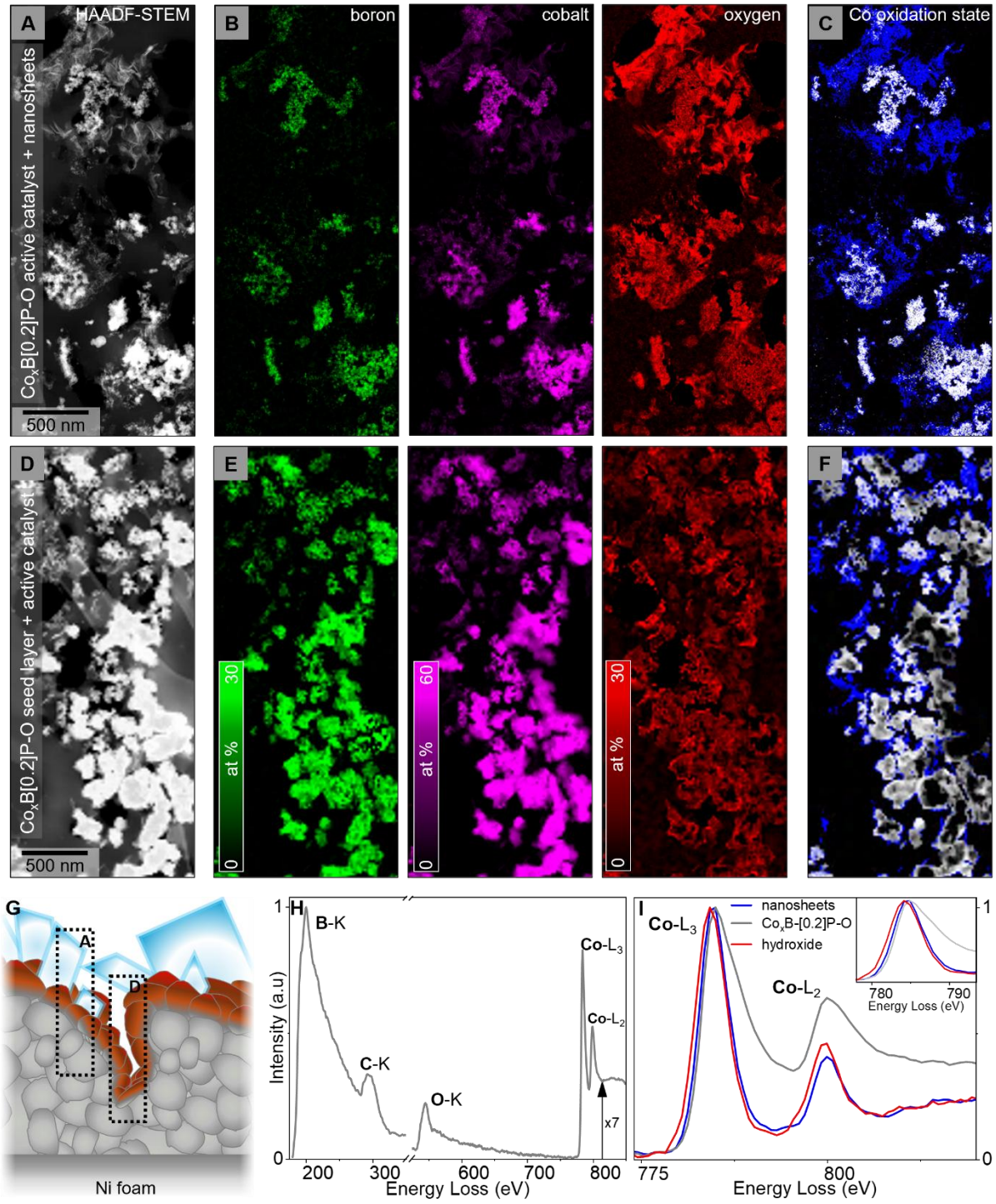

Figure 3: Comprehensive EELS analyses of A-C) active catalyst on D-F) seed layer with G) indicative positions within the electrode: A, D) high-angle annular dark-field scanning TEM (HAADF-STEM) images showing bright seed-layer particles and active catalyst (high density) in contrast to intermediate gray nanosheets (lower density and lower projected thickness), B, E) corresponding B, Co, O element maps (in at. % with P and H concentration omitted due to instrumental and methodological limitations) and C, F), Co oxidation-state maps (colors blue and grey correspond to line colors in I): Co-$L_{2,3}$ spectra), H) overview EEL spectrum, I) representative cobalt $L_{2,3}$ spectra of active catalyst region and nanosheets regions compared to as-synthesized $Co(OH)_2$ reference with shifts in Co L_3 edge as inset.

Cross-sectional TEM samples, prepared by ultramicrotomy, enabled the detailed characterization of the local composition and bonding by STEM electron energy loss spectroscopy (EELS) (Fig. 3). In Fig. 3, both, the seed layer and the active catalyst region are differentiated (Fig. 3 A, D, G). The dense Co_xB-[0.2]P-O particles with active catalyst coating appear bright in the HAADF-STEM images in contrast to the faint nanosheets (Fig. 3 A, D). The systematic co-occurrence of B, Co and a minor concentration of O, as depicted in Fig. 3 B, E, H proves the successful formation of cobalt boride (Co_xB-[0.2]P-O). In contrast, the nanosheets, (upper dataset) consist of Co, higher O concentration and reduced B concentration Both, the Co_xB-[0.2]P-O as well as the nanosheets are linked to specific Co species (cf. Fig. C, F, I, Fig. S11, Fig. S12). Owing the low local concentration and its unsuited shape of the ionization edge in conjunction with the challenging sample geometry, any P distribution could not be derived with the EELS technique (see experimental section). However, the homogeneous incorporation of P is proven by STEM X-ray spectroscopy (Fig. S10) and XPS (Fig. 1 K, Fig. S6).

Furthermore, EELS allows for the separation of the Co oxidation state as particularly the L_3 intensity (in correlation to the L_2 intensity) directly correlates with the number of unoccupied 3d states and is thus a measure for the change in Co oxidation state. The seed-layer particles and active catalyst material show a higher, but mixed oxidation state of Co (Fig. 3 C, F, I) in comparison to the nanosheets. That higher mean oxidation state is not necessarily reflected in an increased L_3/L_2 ratio of the respective peak heights but in a significantly broader L_3 peak (and thus intensity).

Both, the $L_{3,2}$ peak maxima/onsets of the Co_xB-[0.2]P-O (seed layer + active catalyst) are systematically shifted towards higher binding energies by approximately 1 eV compared to the hydroxide reference indicating partial electron transfer to highly electro-negative adjacent species like B and P.[40] While the peak shape of the nanosheets is similar to that of the Co hydroxide reference with a periodic atomic arrangement, the significantly broadened Co L_3 peak of the catalyst indicates strong local variations of the composition and next-neighbor configuration (particularly B/P/O(H)) on the atomic scale and thus varying electronic environments of the active Co species.

This is indicative of a change in the ligand field of the active Co catalyst centers. The incorporation of B and P as phosphite creates a unique ligand environment around Co, which leverages the electron-withdrawing and electron-donating properties of both species.

While B may withdraw or donate (reverse electron transfer) electron density from Co, depending on whether the materials is crystalline or amorphous, P donates electron density

resulting in a complementary interaction with a balanced electronic environment and tailored ligand field, thereby optimizing the overall ad/de-sorption of reactants and facilitating enhanced HER catalytic activity as reflected in the catalytic performance (Fig. 4).

2.3 Electrochemical Performance

The electrocatalytic activity of the electrodes for HER was studied in a common three-electrode cell containing 1.0 M $KOH_{(aq)}$ electrolyte. Graphite and mercury oxide/mercury (HgO/Hg) were used as counter current and reference electrodes respectively (details in SI: electrochemical evaluation section). The properties of the Co_xB-[0.2]P-O as active catalyst coating were determined from comparative *iR*-corrected linear sweep voltammetry (LSV) curves. The LSV curve of Co_xB-[0.2]P-O shows a significant shift toward lower potentials compared to that of both the NF substrate and even a commercial 20% Pt/C catalyst loaded on the NF (Fig. 4 A).

The enhanced catalytic performance of the self-supported Co_xB-[0.2]P-O electrodes is characterized by a very low overpotential of 33 mV (Fig. 4 B, Fig. S14) at the standard geometric current density (η@ 10 mA cm^{-2}). It shows outstanding electrocatalytic performance compared to reported self-supported cobalt-based catalysts (e.g. cobalt-boride-phosphide,[41] cobalt phosphide spheres/cobalt hydroxide nanosheets,[42] cobalt phosphide,[43] cobalt boride,[44] cobalt hydroxide,[45] and cobalt pyrophosphate,[46] cobalt oxide,[47] and other cobalt catalysts[47-48]) for HER in alkaline solution to achieve η@ = 10 mA cm^{-2} (Fig. 4 B). The control sample ($Co(OH)_2$) and the NF substrate required relatively similar values (208 mV for $Co(OH)_2$ and 306 mV for NF at η@ = 10 mA cm^{-2}) as previously reported ones of 228 mV[42] and 182 mV[45] for $Co(OH)_2$, and 252 mV for NF,[41] respectively (Table S1).

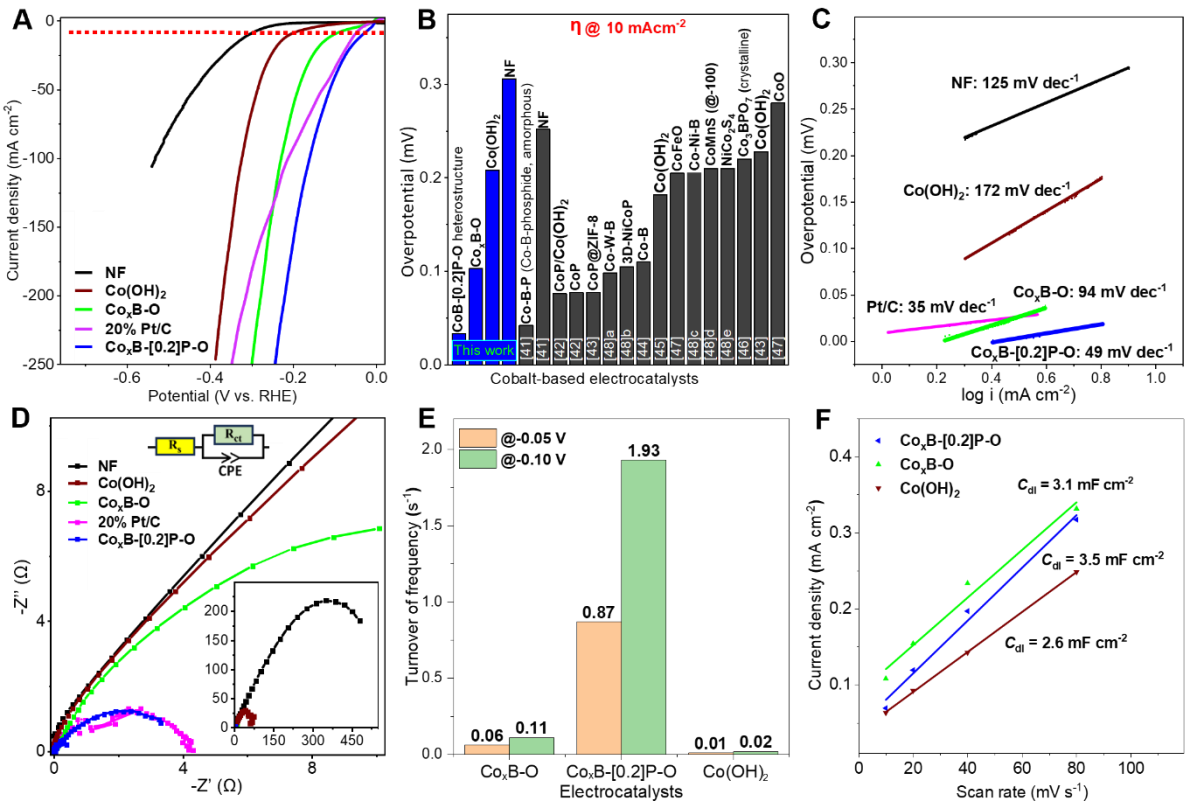

Figure 4: Electrocatalytic performance of catalysts for HER: A) LSV curves for as-fabricated catalysts Co_xB-[0.2]P-O, Co_xB-O, $Co(OH)_2$, commercial Pt/C, and bare NF in 1.0 M KOH, B) comparison of overpotentials of as-prepared Co_xB-[0.2]P-O, Co_xB-O electrocatalysts, and NF to cobalt-based catalysts in alkaline electrolyte solution, C) Tafel slopes and D) EIS Nyquist plots of Co_xB-[0.2]P-O, Co_xB-O, $Co(OH)_2$, commercial Pt/C, and bare NF; insets show the equivalent circuit used for fitting the data and overall Nyquist plot as overview, E) bar graph of the turnover frequency (TOF), F) double-layer capacitance.

The mechanism of HER in an alkaline solution involves an additional step of breaking water molecules to generate protons.[49] This process, therefore, requires extra energy for successful water splitting and causes more sluggish reaction kinetics.[50] This is depicted by the Tafel value for the optimized Co_xB-[0.2]P-O which was observed to be the lowest among the investigated sample series at 49 mV dec^{-1}, which is competitive to Pt/C (35 mV dec^{-1}) (Fig. 4 C). Such a low value infers an enhanced electron-coupled water dissociation step, known to be the rate-determining step for HER in alkaline conditions.[14] This demonstrates that our boron and phosphite-incorporated catalyst (Co_xB-[0.2]P-O) has more efficient HER reaction kinetics relative to $Co(OH)_2$ and Co_xB-O counterparts.

These enhanced reaction kinetics are corroborated by detailed analyses of Nyquist plots retrieved from electrochemical impedance spectroscopy (EIS) measurements (Fig. 4 D). The charge transfer resistance (R_{ct}) values, determined from the radii of the Nyquist plots, were 4.1 Ω, 17.6 Ω, and 69.4 Ω for Co_xB-[0.2]P-O, Co_xB-O (control catalyst), and $Co(OH)_2$ (control catalyst), respectively. Evidently, the optimized boron and phosphite-doped catalyst has a reduced R_{ct} value compared to the counter and control electrocatalysts.

This comparison proves a better adsorption-desorption efficiency of the reactants due to better charge transfer by the reduced binding energy due to the P co-doping.[16] The control catalyst $Co(OH)_2$ exhibits the highest R_{ct} value most likely since this material did not include cobalt-boride or phosphite in the structure. The electronic configuration of cobalt determined by XPS analysis showed that the presence of both B and P of phosphite ensured the tailored chemistry of Co through charge transfer processes, and as a consequence the observed better charge transfer in Co_xB-[0.2]P-O. Among the series of catalysts, only the $Co(OH)_2$ control catalyst exhibits a purely crystalline form (Fig. S8 and Fig. S9), whereas both, Co_xB-[0.2]P-O and Co_xB-O, show mixed amorphous-crystalline heterostructures. We therefore conclude that the chemistry (boron and phosphite incorporation) as well as the co-existence of mixed phases cause the synergistic enhancement of the electron transfer process.

The Co_xB-[0.2]P-O electrocatalyst exhibits by far the highest hydrogen production per active site as demonstrated by a superior TOF value of 0.87 s^{-1} at a voltage of -0.05 V vs. RHE, which is approximately 15 times higher than that of the counter catalyst (Co_xB-O) (Fig. 4 E, Fig. S15). As anticipated from the hierarchical, and rough morphology of the catalyst surface, these electrocatalysts showed relatively similar electrocatalytic surface area (ECSA) which correlates to the double layer capacitance (C_{dl}) values of Co_xB-[0.2]P-O (3.5 mF cm^{-2}), Co_xB-O (3.1 mF cm^{-2}) and $Co(OH)_2$ (2.6 mF cm^{-2}) (Fig. 4 F, Fig. S16). While the ECSA values of the three materials are similar, the TOF measurements provide evidence that the local chemistry of the active site plays a more significant role in promoting the electrocatalytic efficiency of these catalysts.

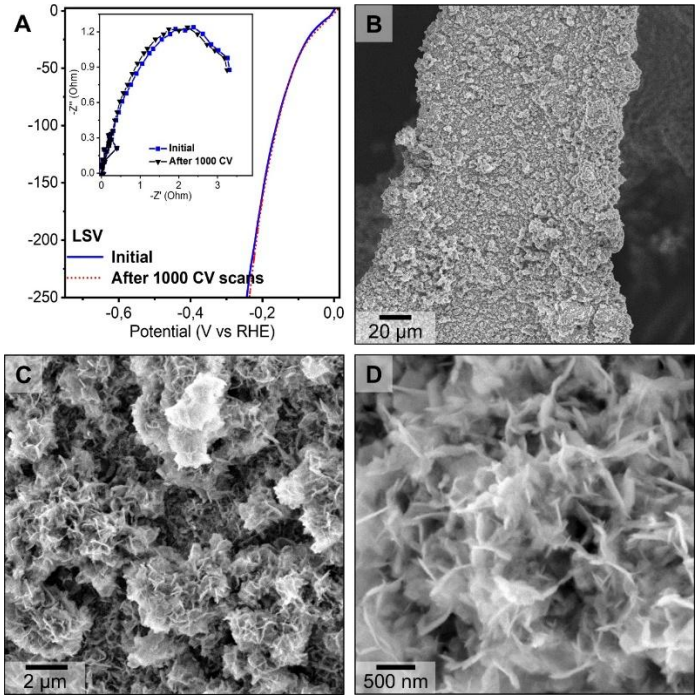

Figure 5: Stability characterization: A) LSV curves before and after 1000 CV scans for the optimized Co_xB-[0.2]P-O catalyst (inset in Fig. 5 A shows overview Nyquist plots)), B-D) SEM images of the electrode after 1000 CV scans.

The Co_xB-[0.2]P-O electrodes show excellent long-term stability after 1000 CV cycles even under alkaline operation conditions as demonstrated by well overlapping LSV curves before and after cycling. Furthermore, the R_{ct} values remain unchanged (Fig. 5 A). Post-operation SEM micrographs further confirm the preservation of the original morphology with only slightly thickened nanosheets (cf. Fig. 1 B-C, Fig. 5 B-D, and Fig. S4) corroborating the excellent mechanical stability during operation.

The strong anchorage of the catalyst even after the stability test on the highly porous and conductive 3D metal substrates provides a major advantage in contrast to conventional drop-casted coatings.[51]

Conclusion

A facile, cost and resource-effective method has been developed to prepare self-supported, highly efficient and long-term stable Pt-like Co_xB-[0.2]P-O electrocatalyst for HER. A comprehensive scale-bridging investigation of the microstructure and chemistry of the complete electrode with emphasis on the active catalyst material has been employed to explain the enhanced electrocatalytic and Pt-competitive HER performance of the electrode in comparison to previous CoxB based catalysts.

Its superior performance is attributed to the complex heterostructured morphology with co-existing crystalline and amorphous phases. Additionally, the modulation of the Co active site chemistry and ligand field due to the incorporation of both, boron and phosphorous species, promotes extrinsic and intrinsic catalytic activity and reduced charge transfer resistance. The comprehensive investigation unraveled the complex interplay between morphology, crystal structure, chemistry and bonding required for the successful production of highly efficient electrocatalysts. This work demonstrated a quite simple synthesis strategy and facilitates the development of more complex earth-abundant transition metal electrocatalysts with high activity toward electrochemical reactions for water splitting.

Supporting Information

Supporting Information is available from XXXX or from the author.

Acknowledgments

JMVN acknowledges funding from the European Union's Horizon 2020 research and innovation program under the Marie Skłodowska-Curie grant agreement No 945422. Part of the study was performed at the DFG-funded Micro-and Nanoanalytics Facility (MNaF) of the University of Siegen (INST 221/131-1) by utilizing its major instrumentation (FEI Talos F200X TEM: DFG INST 221/93-1, DFG INST 221/126-1).

Author contributions

JMVN: project administration, conceptualization, experimental design, material synthesis, physicochemical analysis, data interpretation, manuscript writing, editing and revision, COO: experimental design, TEM investigation, sample preparation, data analysis and interpretation, manuscript writing, editing and revision, JF: STEM tomography and µCT, 3D visualization, MH: SEM-EDXS, NF: XPS, YS: SEM, WSS: original draft revision, editing and figure design, MK: project supervision, project administration, data interpretation, manuscript writing, manuscript review, editing BB: project supervision, project administration, conceptualization, data interpretation, manuscript writing, editing and revision.

Conflict of Interest

The authors declare no conflict of interest.

References

[1] M. Chatenet, B. G. Pollet, D. R. Dekel, F. Dionigi, J. Deseure, P. Millet, R. D. Braatz, M. Z. Bazant, M. Eikerling, I. Staffell, P. Balcombe, Y. Shao-Horn, H. Schäfer, Water electrolysis: from textbook knowledge to the latest scientific strategies and industrial developments, *Chem. Soc. Rev.* **2022**, 51, 4583.

[2] T. Terlouw, L. Rosa, C. Bauer, R. McKenna, Future hydrogen economies imply environmental trade-offs and a supply-demand mismatch, *Nat. Commun.* **2024**, 15, 7043.

[3] Z. W. Seh, J. Kibsgaard, C. F. Dickens, I. Chorkendorff, J. K. Nørskov, T. F. Jaramillo, Combining theory and experiment in electrocatalysis: Insights into materials design, *Science* **2017**, 355.

[4] Y. Aykut, A. Bayrakçeken Yurtcan, Nanostructured electrocatalysts for low-temperature water splitting: A review, *Electrochimica Acta* **2023**, 471, 143335.

[5] a) M. N. Lakhan, A. Hanan, A. Hussain, I. Ali Soomro, Y. Wang, M. Ahmed, U. Aftab, H. Sun, H. Arandiyan, Transition metal-based electrocatalysts for alkaline overall water splitting: advancements, challenges, and perspectives, *Chem. Commun.* **2024**, 60, 5104; b) U. Shahzad, M. Saeed, H. M. Marwani, J. Y. Al-Humaidi, S. u. Rehman, R. H. Althomali, M. M. Rahman, Transition metal-based chalcogenides as electrocatalysts for overall water splitting in hydrogen energy production, *Int. J. hydrog. Energy* **2024**, 65, 215.

[6] Z. Zou, K. Dastafkan, Y. Shao, C. Zhao, Q. Wang, Electrocatalysts for alkaline water electrolysis at ampere-level current densities: a review, *Int. J. Hydrogen Energy.* **2024**, 51, 667.

[7] N. Mahmood, Y. Yao, J.-W. Zhang, L. Pan, X. Zhang, J.-J. Zou, Electrocatalysts for Hydrogen Evolution in Alkaline Electrolytes: Mechanisms, Challenges, and Prospective Solutions, *Adv. Sci.* **2018**, 5, 1700464.

[8] A. A. Feidenhans'l, Y. N. Regmi, C. Wei, D. Xia, J. Kibsgaard, L. A. King, Precious Metal Free Hydrogen Evolution Catalyst Design and Application, *Chemical Reviews* **2024**, 124, 5617.

[9] a) N. Du, C. Roy, R. Peach, M. Turnbull, S. Thiele, C. Bock, Anion-Exchange Membrane Water Electrolyzers, *Chem. Rev.* **2022**, 122, 11830; b) F. Moradi Nafchi, E. Afshari, E. Baniasadi, Anion exchange membrane water electrolysis: Numerical modeling and electrochemical performance analysis, *International Journal of Hydrogen Energy* **2024**, 52, 306.

[10] a) Y. Kang, Y. Tang, L. Zhu, B. Jiang, X. Xu, O. Guselnikova, H. Li, T. Asahi, Y. Yamauchi, Porous Nanoarchitectures of Nonprecious Metal Borides: From Controlled Synthesis to Heterogeneous Catalyst Applications, *ACS Catalysis* **2022**, 12, 14773; b) R. Sun, X. Huang, J. Jiang, W. Xu, S. Zhou, Y. Wei, M. Li, Y. Chen, S. Han, Recent advances in cobalt-based catalysts for efficient electrochemical hydrogen evolution: a review, *Dalton Trans.* **2022**, 51, 15205.

[11] Y. Chen, Q. Li, Y. Lin, J. Liu, J. Pan, J. Hu, X. Xu, Boosting oxygen evolution reaction by FeNi hydroxide-organic framework electrocatalyst toward alkaline water electrolyzer, *Nat. Commun.* **2024**, 15, 7278.

[12] H. Yang, M. Driess, P. W. Menezes, Self-Supported Electrocatalysts for Practical Water Electrolysis, *Adv. Energy Mater.* **2021**, 11, 2102074.

[13] a) S. Gupta, M. K. Patel, A. Miotello, N. Patel, Metal Boride-Based Catalysts for Electrochemical Water-Splitting: A Review, *Adv. Funct. Mater.* **2020**, 30, 1906481; b) E. Lee, B. P. T. Fokwa, Nonprecious Metal Borides: Emerging Electrocatalysts for Hydrogen Production, *Acc. Chem. Res.* **2022**, 55, 56; c) J. Hong, S. Mutalik, P. P. Pescarmona, L. Protesescu, Metal Borides: From Industrial Classics to Versatile

Colloidal Nanocrystals for Energy, Catalysis, and Hard Coatings Applications, *Chem. Mater.* **2024**, 36, 2147.

[14] J. Masa, P. Weide, D. Peeters, I. Sinev, W. Xia, Z. Sun, C. Somsen, M. Muhler, W. Schuhmann, Amorphous Cobalt Boride (Co2B) as a Highly Efficient Nonprecious Catalyst for Electrochemical Water Splitting: Oxygen and Hydrogen Evolution, *Adv. Energy Mater.* **2016**, 6, 1502313.

[15] B. Xu, B. Chong, H. Li, G. Yang, Cobalt incorporation-induced photocatalytic reactivity enhancement in ZnIn2S4 nanosheets for effective hydrogen production, *Chem. Eng. Sci.* **2023**, 280, 118985.

[16] S. Gupta, R. Fernandes, R. Patel, M. Spreitzer, N. Patel, A review of cobalt-based catalysts for sustainable energy and environmental applications, *Applied Catalysis A: General* **2023**, 661, 119254.

[17] a) V. Jose, J. M. V. Nsanzimana, H. Hu, J. Choi, X. Wang, J.-M. Lee, Highly Efficient Oxygen Reduction Reaction Activity of N-Doped Carbon–Cobalt Boride Heterointerfaces, *Adv. Energy Mater.* **2021**, 11, 2100157; b) Y. Zou, Y. Gao, P. Huang, C. Xiang, H. Chu, S. Qiu, E. Yan, F. Xu, L. Sun, Effects of the Preparation Solvent on the Catalytic Properties of Cobalt–Boron Alloy for the Hydrolysis of Alkaline Sodium Borohydride, *Metals* **2017**, 7, 365; c) S. Carenco, D. Portehault, C. Boissière, N. Mézailles, C. Sanchez, Nanoscaled Metal Borides and Phosphides: Recent Developments and Perspectives, *Chem. Rev.* **2013**, 113, 7981.

[18] Y. Wang, D. Wang, K. Qi, Z. Cao, K. Zhang, S. Wu, Preparation and characterization of fishbone-like Co–B nanoparticles with high catalytic activity for hydrogen generation from NaBH4 solution, *Mater. Lett.* **2016**, 165, 147.

[19] S. Gupta, N. Patel, A. Miotello, D. Kothari, Cobalt-boride: an efficient and robust electrocatalyst for hydrogen evolution reaction, *Journal of Power Sources* **2015**, 279, 620.

[20] A. Chunduri, S. Gupta, O. Bapat, A. Bhide, R. Fernandes, M. K. Patel, V. Bambole, A. Miotello, N. Patel, A unique amorphous cobalt-phosphide-boride bifunctional electrocatalyst for enhanced alkaline water-splitting, *Appl. Catal. B* **2019**, 259, 118051.

[21] Y. Chen, Z. Lai, X. Zhang, Z. Fan, Q. He, C. Tan, H. Zhang, Phase engineering of nanomaterials, *Nat Rev Chem* **2020**, 4, 243.

[22] M. Singh, D. C. Cha, T. I. Singh, A. Maibam, D. R. Paudel, D. H. Nam, T. H. Kim, S. Yoo, S. Lee, A critical review on amorphous–crystalline heterostructured electrocatalysts for efficient water splitting, *Mater. Chem. Front.* **2023**, 7, 6254.

[23] Y. Liu, Q. Li, R. Si, G.-D. Li, W. Li, D.-P. Liu, D. Wang, L. Sun, Y. Zhang, X. Zou, Coupling Sub-Nanometric Copper Clusters with Quasi-Amorphous Cobalt Sulfide Yields Efficient and Robust Electrocatalysts for Water Splitting Reaction, *Adv. Mater.* **2017**, 29, 1606200.

[24] Y. Chen, C. Liu, J. Xu, C. Xia, P. Wang, B. Y. Xia, Y. Yan, X. Wang, Key Components and Design Strategy for a Proton Exchange Membrane Water Electrolyzer, *Small Structures* **2023**, 4, 2200130.

[25] H. Lan, J. Wang, L. Cheng, D. Yu, H. Wang, L. Guo, The synthesis and application of crystalline–amorphous hybrid materials, *Chem. Soc. Rev.* **2024**, 53, 684.

[26] a) J. M. V. Nsanzimana, L. Gong, R. Dangol, V. Reddu, V. Jose, B. Y. Xia, Q. Yan, J.-M. Lee, X. Wang, Tailoring of Metal Boride Morphology via Anion for Efficient Water Oxidation, *Adv. Energy Mater.* **2019**, 9, 1901503; b) B. Albert, K. Hofmann, in *Handbook of Solid State Chemistry*, DOI: https://doi.org/10.1002/9783527691036.hsscvol1011, p. 435.

[27] a) M. Lewandowski, M. Bartoszewicz, K. Jaroszewska, G. Djéga-Mariadassou, Transition metal borides of Ni-B (Co-B) as alternative non-precious catalytic materials:

Advances, potentials, and challenges. Short review, *Journal of Industrial and Engineering Chemistry* **2022**, 116, 75; b) H. Sun, J. Meng, L. Jiao, F. Cheng, J. Chen, A review of transition-metal boride/phosphide-based materials for catalytic hydrogen generation from hydrolysis of boron-hydrides, *Inorg. Chem. Front.* **2018**, 5, 760.

[28] Y. Qi, Y. Zhang, L. Yang, Y. Zhao, Y. Zhu, H. Jiang, C. Li, Insights into the activity of nickel boride/nickel heterostructures for efficient methanol electrooxidation, *Nat. Commun.* **2022**, 13, 4602.

[29] Q. Yun, Y. Ge, Z. Shi, J. Liu, X. Wang, A. Zhang, B. Huang, Y. Yao, Q. Luo, L. Zhai, J. Ge, Y. Peng, C. Gong, M. Zhao, Y. Qin, C. Ma, G. Wang, Q. Wa, X. Zhou, Z. Li, S. Li, W. Zhai, H. Yang, Y. Ren, Y. Wang, L. Li, X. Ruan, Y. Wu, B. Chen, Q. Lu, Z. Lai, Q. He, X. Huang, Y. Chen, H. Zhang, Recent Progress on Phase Engineering of Nanomaterials, *Chem. Rev.* **2023**, 123, 13489.

[30] Q. Cai, W. Hong, C. Jian, X. He, W. Liu, Recent Development of Self-Supported Alkaline Hydrogen Evolution Reaction Electrocatalysts for Industrial Electrolyzer, *Adv. Energy Sustainability Res.* **2023**, 4, 2200178.

[31] X. Wang, Y. V. Kolen'ko, X.-Q. Bao, K. Kovnir, L. Liu, One-Step Synthesis of Self-Supported Nickel Phosphide Nanosheet Array Cathodes for Efficient Electrocatalytic Hydrogen Generation, *Angew. Chem. Int. Ed.* **2015**, 54, 8188.

[32] N. Patel, A. Miotello, Progress in Co–B related catalyst for hydrogen production by hydrolysis of boron-hydrides: A review and the perspectives to substitute noble metals, *Int. J. Hydrog. Energy* **2015**, 40, 1429.

[33] a) O. V. Netskina, D. I. Kochubey, I. P. Prosvirin, S. E. Malykhin, O. V. Komova, V. V. Kanazhevskiy, Y. G. Chukalkin, V. I. Bobrovskii, D. G. Kellerman, A. V. Ishchenko, V. I. Simagina, Cobalt-boron catalyst for NaBH4 hydrolysis: The state of the active component forming from cobalt chloride in a reaction medium, *Molecular Catalysis* **2017**, 441, 100; b) J. Lu, D. B. Dreisinger, W. C. Cooper, Cobalt precipitation by reduction with sodium borohydride, *Hydrometallurgy* **1997**, 45, 305.

[34] M. C. Biesinger, B. P. Payne, A. P. Grosvenor, L. W. M. Lau, A. R. Gerson, R. S. C. Smart, Resolving surface chemical states in XPS analysis of first row transition metals, oxides and hydroxides: Cr, Mn, Fe, Co and Ni, *Applied Surface Science* **2011**, 257, 2717.

[35] P. W. Menezes, C. Panda, S. Loos, F. Bunschei-Bruns, C. Walter, M. Schwarze, X. Deng, H. Dau, M. Driess, A structurally versatile nickel phosphite acting as a robust bifunctional electrocatalyst for overall water splitting, *Energy Environ. Sci.* **2018**, 11, 1287.

[36] Y. Liu, J. Zhang, X. Li, Z. Zeng, X. Cheng, Y. Wang, M. Pan, Phosphorous Modified Metal Boride as High Efficiency HERElectrocatalyst, *Int. J. Electrochem. Sci.* **2019**, 14, 6123.

[37] a) Y. Tian, X. Lian, Y. Wu, W. Guo, S. Wang, The morphology controlled growth of Co11(HPO3)8(OH)6 on nickel foams for quasi-solid-state supercapacitor applications, *CrystEngComm* **2020**, 22, 5218; b) H. Pang, C. Wei, Y. Ma, S. Zhao, G. Li, J. Zhang, J. Chen, S. Li, Nickel Phosphite Superstructures Assembled by Nanotubes: Original Application for Effective Electrode Materials of Supercapacitors, *ChemPlusChem* **2013**, 78, 546.

[38] G. Gouget, D. P. Debecker, A. Kim, G. Olivieri, J.-J. Gallet, F. Bournel, C. Thomas, O. Ersen, S. Moldovan, C. Sanchez, S. Carenco, D. Portehault, In Situ Solid–Gas Reactivity of Nanoscaled Metal Borides from Molten Salt Synthesis, *Inorg. Chem.* **2017**, 56, 9225.

[39] Z. Wang, X. Ke, M. Sui, Recent Progress on Revealing 3D Structure of Electrocatalysts Using Advanced 3D Electron Tomography: A Mini Review, *Front. Chem.* **2022**, 10, 872117.
[40] H. Tan, J. Verbeeck, A. Abakumov, G. Van Tendeloo, Oxidation state and chemical shift investigation in transition metal oxides by EELS, *Ultramicroscopy* **2012**, 116, 24.
[41] H. Sun, X. Xu, Z. Yan, X. Chen, L. Jiao, F. Cheng, J. Chen, Superhydrophilic amorphous Co–B–P nanosheet electrocatalysts with Pt-like activity and durability for the hydrogen evolution reaction, *J. Mater. Chem. A* **2018**, 6, 22062.
[42] Y. Chu, D. Wang, J. Wang, S. Zha, M. Wu, C. Liu, W. Wang, N. Mitsuzaki, Z. Chen, Synergistic Interfacial Engineering of Heterostructured Cobalt Phosphide Spheres/Cobalt Hydroxide Nanosheets for Overall Water Splitting, *Inorg. Chem.* **2023**, 62, 18189.
[43] H. Wang, L. Zhang, W. Zhang, S. Sun, S. Yao, Highly Efficient Spatial Three-Level CoP@ZIF-8/pNF Based on Modified Porous NF as Dual Functional Electrocatalyst for Water Splitting, *Nanomaterials (Basel)* **2023**, 13, 1386.
[44] Z. Chen, Q. Kang, G. Cao, N. Xu, H. Dai, P. Wang, Study of cobalt boride-derived electrocatalysts for overall water splitting, *Int. J. Hydrog. Energy* **2018**, 43, 6076.
[45] S. Sriram, S. Mathi, B. Vishnu, J. Jayabharathi, Entwined Co(OH)2 In Situ Anchoring on 3D Nickel Foam with Phenomenal Bifunctional Activity in Overall Water Splitting, *Energy Fuels* **2022**, 36, 7006.
[46] E. Ülker, S. S. Akbari, F. Karadas, Cobalt borophosphate on nickel foam as an electrocatalyst for water splitting, *Mater. Chem. Phys.* **2022**, 288, 126390.
[47] H. A. Bandal, A. R. Jadhav, A. H. Tamboli, H. Kim, Bimetallic iron cobalt oxide self-supported on Ni-Foam: An efficient bifunctional electrocatalyst for oxygen and hydrogen evolution reaction, *Electrochimica Acta* **2017**, 249, 253.
[48] a) G.-X. Cao, N. Xu, Z.-J. Chen, Q. Kang, H.-B. Dai, P. Wang, Cobalt-Tungsten-Boron as an Active Electrocatalyst for Water Electrolysis, *ChemistrySelect* **2017**, 2, 6187; b) B. Ma, Z. Yang, Y. Chen, Z. Yuan, Nickel cobalt phosphide with three-dimensional nanostructure as a highly efficient electrocatalyst for hydrogen evolution reaction in both acidic and alkaline electrolytes, *Nano Res.* **2019**, 12, 375; c) N. Xu, G. Cao, Z. Chen, Q. Kang, H. Dai, P. Wang, Cobalt nickel boride as an active electrocatalyst for water splitting, *J. Mater. Chem. A* **2017**, 5, 12379;
d) J. Li, W. Xu, J. Luo, D. Zhou, D. Zhang, L. Wei, P. Xu, D. Yuan, Synthesis of 3D Hexagram-Like Cobalt–Manganese Sulfides Nanosheets Grown on Nickel Foam: A Bifunctional Electrocatalyst for Overall Water Splitting, *Nano-Micro Lett.* **2017**, 10, 6; e) A. Sivanantham, P. Ganesan, S. Shanmugam, Hierarchical NiCo2S4 Nanowire Arrays Supported on Ni Foam: An Efficient and Durable Bifunctional Electrocatalyst for Oxygen and Hydrogen Evolution Reactions, *Adv. Funct. Mater.* **2016**, 26, 4661.
[49] J. Kundu, H. J. Kim, M. Li, H. Huang, S.-I. Choi, Recent advances in mechanistic understanding and catalyst design for alkaline hydrogen evolution reactions, *Materials Chemistry Frontiers* **2023**, 7, 6366.
[50] N. Mahmood, Y. Yao, J.-W. Zhang, L. Pan, X. Zhang, J.-J. Zou, Electrocatalysts for Hydrogen Evolution in Alkaline Electrolytes: Mechanisms, Challenges, and Prospective Solutions, *Adv. Sci.* **2018**, 5, 1700464.
[51] H. Sun, Z. Yan, F. Liu, W. Xu, F. Cheng, J. Chen, Self-Supported Transition-Metal-Based Electrocatalysts for Hydrogen and Oxygen Evolution, *Adv. Mater.* **2020**, 32, 1806326.